Thermal and Crystallization Properties of the Alternated Tere/Iso PEKK Copolymer: Importance in High-Temperature Laser Sintering

Alexis Cherri, Ilias Iliopoulos, Gilles Régnier, Benoit Brulé, Guillaume Lé, and Sylvie Tencé-Girault*

ABSTRACT: High-temperature laser sintering (HT-LS) is a very promising additive manufacturing process for the production of parts of complex geometry for highly demanding applications. Poly(aryl ether ketone) polymers such as poly(ether ketone), poly(ether ether ketone), and poly(ether ketone ketone) (PEKK) have attracted increasing interest during the last decade for use in HT-LS. Among them, PEKK offers the advantage of exhibiting tunable melting temperature and crystallization rate due to its copolymer structure. Indeed, PEKK is synthesized by Friedel−Crafts polyacylation condensation of diphenyl ether with terephthaloyl chloride (T units) and isophthaloyl chloride (I units). In this work, we focus on a specific member of the PEKK family having a regular alternated T/I structure, PEKK 50/50, and study its isothermal crystallization from the melt at various crystallization temperatures (T_C), from 200 °C to 290 °C. A quantitative analysis based on X-ray scattering and differential scanning calorimetry experiments is performed. Primary crystallization dominates the process with a half-time of crystallization higher than 6 min and an Avrami exponent between 2.2 and 3. Stacks of periodic crystalline lamellae are first created, followed by lateral growth of these crystalline lamellae, leading to a gradual increase of the weight crystallinity. Crystalline form I, with traces of form III, is mostly observed regardless of T_C. The amount and perfection of the crystalline phase increase with T_C. The crystalline state achieved, as well as the thermal and rheological behavior of PEKK 50/50 during crystallization at high T_C (~280−290 °C), are promising for use in HT-LS manufacturing.

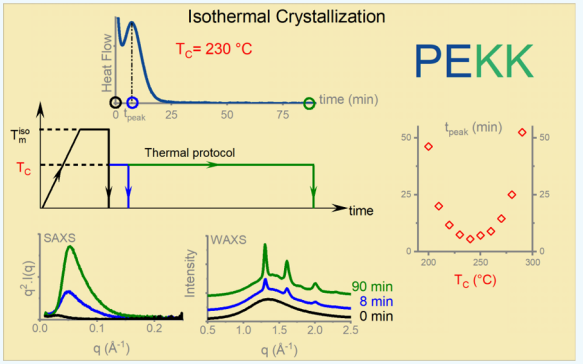

KEYWORDS: *PEKK, crystallization kinetics, DSC, SAXS−WAXS, laser sintering*

1. INTRODUCTION

Poly(aryl ether ketone) (PAEK) is a family of high-performance semicrystalline thermoplastic polymers composed of phenyl units connected by ether or ketone groups. They are used in highly demanding applications such as, for example, in aerospace, automotive, and oil and gas industries. They present excellent thermomechanical properties and solvent resistance and are inherently fire-resistant.[1,2]

When comparing PAEK polymers having a fully para-phenyl chain structure, their glass-transition temperature (T_g) and melting temperature (T_m) increase continuously with the increase of the ketone to ether ratio due, respectively, to an increase in the stiffness of the macromolecular chain and to an enhancement of the crystal packing efficiency.[3] For poly(ether ether ketone) (PEEK) (33% ketone), T_g = 133 °C[3] and T_m = 335 °C;[4] for PEK (50% ketone), T_g = 150 °C[3] and T_m = 365 °C;[4] for PEKEKK (60% ketone), T_g = 153 °C[3] and T_m = 370 °C;[4] and for poly(ether ketone ketone) (PEKK) (67% ketone), T_g = 165 °C[3] and T_m = 385 °C.[4] All these polymers can crystallize with the same orthorhombic crystal cell as PEEK, although the b and c cell parameters increase with the amount of ketone.[4]

PEEK and PEKK are the most known and studied members of the PAEK family and are industrially available. An advantage of PEKK over PEEK is the possibility to tune T_m while keeping T_g almost constant. This is achieved by replacing a part of the para-phenyl units by meta-phenyl ones that break the regularity of the polymer chain. PEKKs are prepared by Friedel−Crafts polyacylation condensation of diphenylene ether (D) with terephthaloyl (T) and/or isophthaloyl (I) chlorides in a two-step process.[5−7] The first step consists of the synthesis of 1,4- or 1,3-bis(4-phenoxybenzoyl)benzenes, respectively, referred to as DTD or DID (Figures 1 and S1). The second step is the synthesis of the final polymer by reacting DTD (or DID) with the appropriate mixture of T and I chlorides. Therefore, PEKKs can be viewed as random copolymers consisting of TT and TI diads when 50% < *T* % < 100% (Figure 1) and as

Received: January 17, 2022
Accepted: February 25, 2022
Published: March 8, 2022

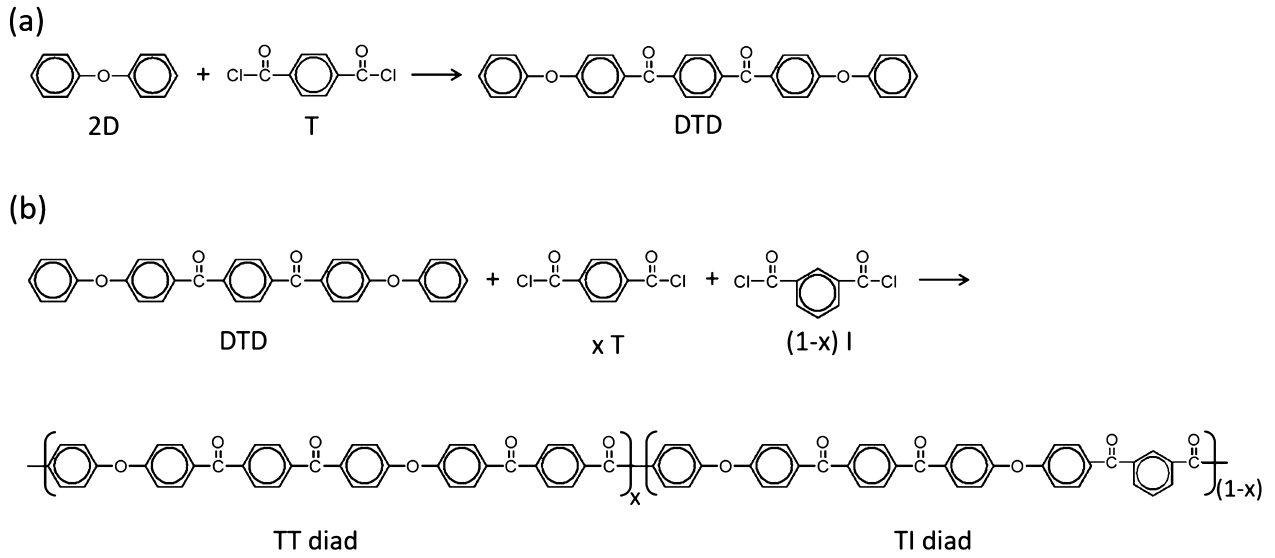

Figure 1. Two-step synthesis of PEKKs by Friedel–Crafts polyacylation condensation for compositions T/I ≥ 50/50: (a) synthesis of DTD by reaction of diphenylene ether (D) with terephthaloyl chloride (T) and (b) synthesis of PEKK copolymers by reaction of DTD with a mixture of terephthaloyl (T) and isophthaloyl (I) chlorides. The alternated PEKK 50/50 copolymer is obtained for $x = 0$. Copolymers with $T/I < 50/50$ are shown in Figure S1.

copolymers consisting of II and TI diads when 0% < *T* % < 50% (Figure S1). On the other hand, PEKK 50/50 consisting of equal amounts of T and I units (50% T and 50% I) can be seen as an alternated copolymer (with a regular chain structure) or even as a homopolymer consisting of TI diads only. Moreover, its synthesis is simpler, requiring addition of only one phthaloyl chloride in the second step of Figure 1. Finally, the two extreme members of the PEKK family, PEKK 100/0 (100% T) and PEKK 0/100 (100% I), are homopolymers.

The thermal and structural properties of PEKKs have been extensively studied by Hsiao et al. and Gardner et al. in the 90s.[3,8] Their T_g varies between 147 and 165 °C and their T_m varies between 270 and ∼410 °C depending on the *T*/*I* ratio.[3,8] The PEKK 100/0 homopolymer has the highest T_g and T_m (165 and ∼410 °C, respectively). Although appealing for high-temperature demanding applications, PEKK 100/0 is very difficult to process because its T_m is close to the degradation temperature.[3] Incorporation of isophthaloyl (I) units in the PEKK chain reduces T_m and facilitates processing. On the other hand, incorporation of isophthaloyl units significantly slows down the crystallization kinetics, which is very fast for PEKK 100/0, and decreases up to 4 orders of magnitude for PEKK 30/70, while the maximum crystallization rate is observed at around 240 °C independent of the T/I ratio.[3,8] These evolutions are attributed to the increase of the chain flexibility in the melt and to the introduction of symmetry defects within the crystal as the isophthaloyl unit (I-isomer) content increases.[3]

The commercially available PEKKs are copolymers with T/I ratios of 80/20, 70/30, and 60/40. They are provided by Arkema as Kepstan 8000, 7000, and 6000, respectively.[9] Each of them is designed for different types of applications and processes. PEKK 80/20 retains its mechanical properties at high temperatures and is used in stock shape extrusion and injection molding.[10] PEKK 70/30 is used as a matrix in thermoplastic composites (prepreg, UD tapes)[11] and for film extrusion.[10] PEKK 60/40 has the lowest crystallization rate and is especially designed for additive manufacturing processes such as laser sintering (LS)[12,13] and fused filament fabrication.[14] For successful use in all these applications, it is important to know and control the crystallization kinetics, the nature and stability of the crystalline phases, and the overall crystallinity of the processed parts. This allows the optimization and mastering of the final properties of the processed parts.

Although PEKK crystallizes in the same orthorhombic cell as PEEK, it additionally exhibits crystal polymorphism that depends on the T/I ratio and crystallization conditions such as the crystallization temperature and the initial state (as-synthesized, amorphous glassy or melt).[6] Most of the members of the PEKK family exhibit two crystalline phases (form I and form II), which differ in their chain packing. Gardner et al. reported that the phenyl–phenyl interactions are edge-to-face in form I and face-to-face in form II.[3] A peculiar member of the PEKK family is PEKK 50/50, which has a regular structure consisting of alternated T and I units. Despite its structural regularity, PEKK 50/50 exhibits an even richer polymorphism with an extra crystalline phase (form III) and a complex thermal behavior with enthalpic events occurring between 260 and 340 °C.[15,16] On the other hand, PEKK 50/50 exhibits some similarities to PEKK 60/40 in terms of melting and crystallization temperatures and crystallization kinetics, making it a good candidate as a high-performance thermoplastic material for additive manufacturing and in particular for high-temperature laser sintering (HT-LS).

In this work, we focus on the behavior of PEKK 50/50, in particular on its crystallization from the melt by studying the crystallization kinetics over the full temperature window (between T_g and T_m) and analyzing the crystalline forms as a function of crystallization temperature (T_C) and crystallization time (t_C). To this end, we use three techniques: differential scanning calorimetry (DSC), X-ray diffraction at wide and small angles (WAXS and SAXS), and rheology. We compare our results with those published recently for other PEKK copolymers[17−19] and discuss the relevance of this specific PEKK for HT-LS.

2. EXPERIMENTAL SECTION

2.1. Materials. PEKK studied in this work is an alternated PEKK 50/50 copolymer (Figure 1). It consists of coarse grain size powder provided by Arkema. The as-received sample underwent a drying step at around 180 °C after synthesis. The thermal treatments (melt crystallization or annealing), applied to the as-received PEKK powder in a DSC oven are detailed in Section 2.2. The full list of the samples is given in Supporting Information Table S1.

2.2. Differential Scanning Calorimetry. Isothermal crystallization from the melt was carried out with a TA instrument Q1000, equipped with an RCS90 intracooler, on samples of about 5−7 mg. Samples were first heated at 380 °C (T_m^{iso}) (around 30 °C higher than the melting temperature offset) during 5 min to erase polymer thermal history. Samples were then cooled at 40 °C·min^{-1} to the crystallization temperature T_C and held at this temperature during the crystallization time t_C. For full crystallization, $t_C = t_C^{full}$ is chosen higher than 5 times the time to reach the maximum of the exothermic signal.[20] After t_C^{full}, no significant evolution of the heat flow was measured. Finally, the polymer is cooled below the glass-transition temperature (T_g) at 40 °C·min^{-1} (the highest effective cooling rate achievable with the TA instrument Q1000/RCS90 intracooler). For each sample, a final heating was carried out until 380 at 10 °C·min^{-1} to analyze crystals formed during the isothermal crystallization. This protocol is shown Figure 2.

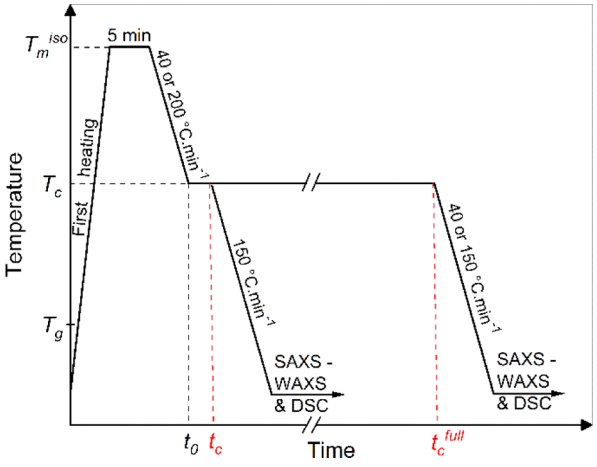

Figure 2. Protocols to study isothermal crystallization and to prepare samples crystallized at various T_C and t_C for SAXS−WAXS and DSC analysis.

Partially crystallized samples, held at T_C for time $t_C < t_C^{full}$, were also prepared for SAXS−WAXS analysis. These samples were prepared using the oven of a PerkinElmer 8500 DSC apparatus, which can achieve high cooling rates, allowing partially crystallized samples to be quenched. After the 5 min isotherm at T_m^{iso}, samples were cooled at 200 °C·min^{-1} to the crystallization temperature T_C and held at this temperature during various times $t_C < t_C^{full}$ before quenching at 150 °C·min^{-1} to a temperature below T_g (in this temperature range, 150 °C is the highest effective cooling rate achievable with the PerkinElmer 8500) (Figure 2). For each crystallization state (T_C and t_C), two samples were prepared: one for use in the SAXS−WAXS experiment and the other for DSC heating scan to 380 at 40 °C·min^{-1} in order to analyze its melting behavior. Samples melt-crystallized at T_C during t_C are named MC-T_C-t_C. For example, PEKK crystallized from the melt at 260 °C during 90 min is named MC-260-90.

Some annealed samples were also prepared, from the as-received powder, at various annealing temperatures (T_{An}) during various times (t_{An}). These samples were named An-T_{An}-t_{An}. The full list of the samples, melt-crystallized or annealed, is given in Supporting Information Table S1.

2.3. Simultaneous SAXS−WAXS Experiments. Simultaneous SAXS−WAXS experiments were performed on a Nano-inXider SW (Xenocs) system in the transmission mode using Cu Kα radiation (λ = 1.54 Å) from an X-ray microsource (GeniX3D) operating at 50 kV−0.6 mA (30 W). Scattering patterns were collected using the combination of two detectors, Pilatus3 (Dectris), operating simultaneously in SAXS and WAXS positions. The entire system, from the source to the sample and to the two detectors, is under vacuum. The distances between the sample and the SAXS and WAXS detectors are fixed, allowing a continuous q range between 0.01 and 4.2 Å^{-1} (2θ range between 0.15 and 62°). The X-ray beam spot has a diameter of 800 μm. SAXS and WAXS patterns were recorded during 600 s. The corrected two-dimensional data were azimuthally integrated using Foxtrot data reduction software (Version 3.4.9)[21] and then normalized to the number of transmitted photons and to the sample thickness. After subtraction of a blank (spectra without the sample), the SAXS and WAXS profiles were treated to extract structural quantitative values. The scattering vector q is defined as $q = 4\pi\frac{\sin\theta}{\lambda}$, where 2θ is the Bragg angle.

WAXS spectra were fitted using the Fityk 0.9.8 software[22] in a wide q range [0.36, 4.1 Å^{-1}] (2θ range [5, 60°]). With this software, the WAXS spectra were decomposed into crystalline and amorphous contributions. The crystalline peaks are associated with sharp peaks, located at the Bragg angle $2\theta_{hkl}$, while broad peaks fit the amorphous signal. The interplanar distance d_{hkl} [distance between the (hkl) planes into the crystalline phase] was deduced from the Bragg angle $2\theta_{hkl}$ using the Bragg law

$$d_{hkl} = \lambda/2\sin\theta_{hkl} = 2\pi/q_{hkl} \quad (1)$$

Using the peak-fitting method previously described,[19] an absolute weight crystallinity χ_c^w can be calculated, for isotropic samples, using the following equation

$$\chi_c^w = \frac{A_c}{A_c + A_a} \quad (2)$$

Here, A_c is the sum of the integrated intensities of the crystalline peaks, and A_a is the total integrated intensity of the amorphous halo. A_c and A_a are calculated in the required wide q range from 0.36 to 4.1 Å^{-1}.[19] The extension of crystal domains, D_{hkl}, perpendicular to (hkl) planes is deduced from the full width at half-maximum of the (hkl) Bragg peak using the Scherrer formula[23]

$$D_{hkl} = \frac{0.9 \times \lambda}{\Delta 2\theta_{hkl}^{cor} \times \cos\theta_{hkl}} = \frac{2\pi \times 0.9}{\Delta q_{hkl}^{cor}} \quad (3)$$

where $\Delta 2\theta_{hkl}^{cor}$ (Δq_{hkl}^{cor}) is the full width corrected for the instrumental resolution.[24]

In semicrystalline polymers, crystals grow to form crystalline lamellae. These lamellae are periodically organized, and the amorphous phase is intercalated between the crystalline lamellae. A correlation peak characterizing this periodic organization can be observed in SAXS spectra. The average period of this organization, L_P, named the ≪long period≫ is deduced from the position, q_{max}, of this correlation peak

$$L_P = \frac{2\pi}{q_{max}} \quad (4)$$

While the integrated intensity of this correlation peak gives the invariant, for an ideal semicrystalline polymers fully organized in stacks of crystalline lamellae and the amorphous phase periodically organized, the invariant is

$$\text{Inv} = \int_0^\infty q^2 \cdot I(q)\mathrm{d}q \propto (\rho_c - \rho_a)^2 \cdot \chi_c^L(1 - \chi_c^L) \quad (5)$$

where ρ_c and ρ_a are the densities of the crystalline and amorphous phases, respectively, and χ_c^L is the linear crystallinity, defined as

$$\chi_c^L = \frac{L_C}{L_P} \quad (6)$$

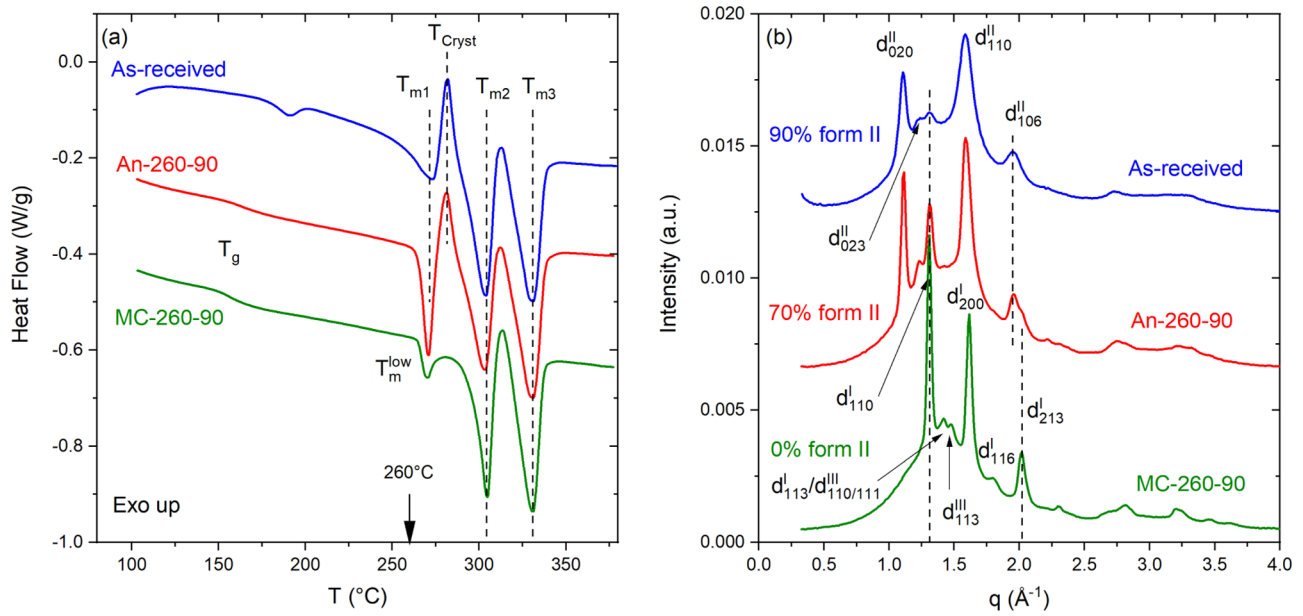

Figure 3. (a) DSC thermograms first heating at 10 °C/min and (b) WAXS spectra of PEKK 50/50 As-received, annealed 90 min at 260 °C (An-260-90), and crystallized from the melt 90 min at 260 °C (MC-260-90).

If all the crystalline and the amorphous phases are localized into the lamellar stacks, that is, if there is no amorphous region lying outside of the lamellar stacks, the linear crystallinity coincides with the total volume crystallinity $\chi_c^V = V_C/V_{total}$. The volume crystallinity can be calculated from the weight crystallinity χ_c^w multiplying by ρ/ρ_c, where ρ is the total density of the material.

In this study, a quantitative analysis of SAXS profiles was performed and the one-dimensional electron density correlation function, $K(z)$, along the lamella normal direction z, was calculated.[25] Using the Strobl and Schneider method, the linear crystallinity χ_c^L is deduced from $K(z = 0)$ and A. $-A$ is the ordinate of the first minimum, named the ≪base line≫ in ref 25

$$\chi_c^L = \frac{A}{A + K(z = 0)} \tag{7}$$

The reader can also refer to Figure S2, where the normalized correlation function, $K(z)/K(z = 0)$, has been plotted. Following the original publications,[25,26] the crystalline lamella thickness (L_C) is also deduced. The thickness of the amorphous phase in between two crystalline lamellae is $L_a = L_P - L_C$. The calculation of $K(z)$ was integrated in the XSACT software,[27] and the procedure used to calculate χ_c^L and L_C is discussed in the Supporting Information (Figures S2 and S3).

2.4. Rheology Measurements. Rheology measurements were run on an HR20 rheometer (TA Instruments) equipped with an ETC oven and a liquid nitrogen cooling device. They consisted in measuring the evolution of complex viscosity (η^*), storage modulus (G'), and loss modulus (G'') during crystallization from the melt using a 25 mm parallel plate geometry. Automatic gap correction was applied when varying the temperature between 380 °C and the crystallization temperature (280 °C). The experiments were run in the linear viscoelastic regime at 1% strain rate and an angular frequency of 1 rad·s^{-1}.

First, the polymer powder was dried in an oven at 120 °C for at least 48 h. The required amount of powder was then compressed in a homemade mold using a manual press to form a disc of a diameter of 25 mm and a thickness of ∼1.5 mm. The compressed powder disc was positioned on the lower plateau of the rheometer geometry, which was preheated at 380 °C, and the oven was closed. Once the temperature stabilized again at 380 °C, the upper plateau of the geometry was lowered until reaching a gap position of 0.6 mm and measurements started. After 5 min equilibration at 380 °C, the temperature was decreased to 280 °C (5 min cooling ramp) and η^*, G', and G'' were recorded until the sample became solid-like ($G' > G''$).

3. RESULTS

3.1. Polymorphism in PEKK 50/50. As mentioned in the Introduction, PEKK is known for its numerous crystalline forms. In Figure 3, we compare DSC thermograms (Figure 3a) and WAXS spectra (Figure 3b) of PEKK 50/50 powder having undergone different thermal treatments: annealed 90 min at 260 °C (An-260-90), melt-crystallized 90 min at 260 °C (MC-260-90), and no thermal treatment (As-received).

The first observation in Figure 3a is the complexity of thermograms with various melting and crystallization peaks, already reported in the literature.[3,15] We observe three main melting peaks in a large temperature range, between 250 and 350 °C. For As-received and annealed samples, the first endotherm, at T_{m1}, is followed by a crystallization peak at T_{Cryst} ∼ 282 °C and two melting peaks located at T_{m2} and at T_{m3}. On the DSC trace of the MC-260-90 sample, no crystallization peak is detected at 282 °C, and the melting endotherm at 270 °C could be attributed to the low endotherm peak, usually observed for these polymers at $T_m^{low} \cong T_C + 10$ °C.[3,28,29,19] The same melting temperatures, T_{m2} and T_{m3}, are measured for the three samples, respectively, at 305 and 331 °C. Glass transition could be observed for melt-crystallized and annealed samples, respectively, at $T_g = 160.6$ °C and at $T_g = 161.5$ °C. For the As-received sample, T_g is not detectable, probably disturbed by the drying step at the origin of the small endothermic peak at 190 °C (see Section 2.1, Materials).

From WAXS diffractograms (Figure 3b), we identify the three different phases (form I, form II, and form III) already discussed in the Introduction section. The theoretical Bragg peak positions of the three crystalline phases, calculated from published cell parameters,[15] are reported in the Supporting Information (Table S2). By comparing these theoretical positions with the spectra of Figure 3, we conclude that form II is mainly observed for the As-received and An-260-90 samples and it is totally missing for MC-260-90. Furthermore,

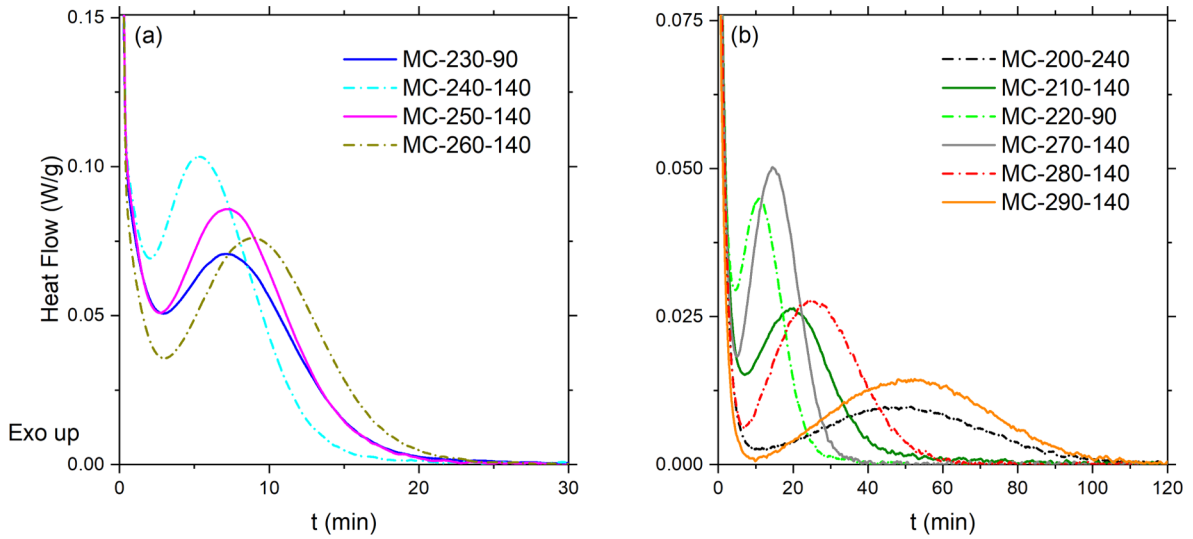

Figure 4. Isothermal crystallization curves of PEKK 50/50 for crystallization temperatures from 200 to 290 °C. The crystallization time scale is adapted to the kinetics: (a) fast kinetics and (b) slow kinetics.

in the latter sample, two small peaks associated to form III are detected in addition to those of form I. The form II fraction reported in Figure 3b is deduced following the procedure published previously.[19]

3.2. Crystallization Kinetics. *3.2.1. DSC Experiments.* Isothermal DSC scans obtained according to the protocol described in Figure 2 are reported Figure 4. During the first minutes of the crystallization isotherm, the beginning of the crystallization peak is hidden by the drop of heat flow due to instrumental thermal inertia.[17] As will be explained later and in the Supporting Information, to overcome this problem, the first experimental points will not be taken into account for the numerical treatment. The origin of the time scale, $t_C = 0$, was chosen at the beginning of the isotherm at t_0 (Figure 2). As our DSC isothermal exotherms are completely recorded until t_C^{full} (ranging from 90 to 240 min), we were able to subtract a horizontal baseline, extrapolated from the flat portion of the curve at the end of the crystallization around t_C^{full} (Figure S4a).[20]

As observed in Figure 4, the exothermic peak evolves significantly with T_C, with the peak time (time corresponding to the peak maximum) ranging from 5 to 50 min for T_C varying in a wide temperature range from 200 °C (T_g + 40 °C) to 290 °C (T_{m3}−40 °C). The lowest crystallization rates are observed for the extreme crystallization temperatures of 200 and 290 °C, while the highest rates are observed for intermediate temperatures around 240 °C.

These crystallization isotherms represent the conversion of the amorphous volume to crystal domains, including nucleation and crystal growth, in terms of both rates and geometries. The treatment of crystallization kinetics remains based on the Avrami approach, even if specific developments for polymer crystallization have been proposed by many authors.[30−34] The Avrami equation is written as

$$\alpha(t) = 1 - \exp(-K \cdot t^n) \tag{8}$$

where $\alpha(t)$ is the relative crystallinity at time t, K is the crystallization rate constant, and n is the Avrami exponent.

For polymers, the dual crystallization mechanism[35] or primary followed by secondary crystallizations are reported in order to explain the observation of two crystallization stages associated with two Avrami exponents.[31,36,37] For example, two independent Avrami crystallization processes, with two exponents, n_1 and n_2, are combined in parallel or in series to explain the PEEK crystallization.[35] In other models, the secondary crystallization kinetics is assumed to be constrained by the advancement of the primary crystallization.[31,38] In these later models, the radial growth of spherulites is associated with primary crystallization, while secondary crystallization takes place within spherulites. In front of this multitude of models, we choose to analyze our DSC data according to the Hillier model[31] already applied to PEKK crystallization.[17,18] In this model, the relative crystallinity $\alpha(t)$ can be expressed as a function of the primary $\alpha_1(t)$ and secondary $\alpha_2(t)$ crystallization

$$\alpha(t) = w_1\alpha_1(t) + w_2\alpha_2(t) \tag{9}$$

$$\alpha_1(t) = 1 - \exp(-K_1 \cdot t^{n_1}) \tag{10}$$

$$\alpha_2(t) = K_2 \int_0^t [1 - \exp(-K_1 \cdot \theta^{n_1})] \cdot \exp[-K_2(t - \theta)] \mathrm{d}\theta \tag{11}$$

where K_1 and K_2 are the crystallization rate constants, w_1 and w_2 are the weight fractions of primary and secondary crystallization, respectively, and n_1 is the Avrami exponent of the primary crystallization. At any time, we have $w_1 + w_2 = 1$. In the model considered here, the secondary crystallization is a first-order process ($n_2 = 1$).[31] We use this model to fit the crystallization heat flow $\mathrm{d}H(t)/\mathrm{d}t$ measured by DSC (Figure 4)

$$\frac{\mathrm{d}H(t)}{\mathrm{d}t} = \Delta H_C \cdot \frac{\mathrm{d}\alpha(t)}{\mathrm{d}t} \tag{12}$$

$$\frac{\mathrm{d}\alpha(t)}{\mathrm{d}t} = w_1 K_1 n_1 t^{n_1 - 1} \exp(-K_1 \cdot t^{n_1}) + (1 - w_1) K_2 [1 - \exp(-K_1 \cdot t^{n_1})] - (1 - w_1) K_2^2 \int_0^t [1 - \exp(-K_1 \cdot \theta^{n_1})] \cdot \exp[-K_2(t - \theta)] \mathrm{d}\theta \tag{13}$$

where ΔH_C is the isothermal crystallization enthalpy.

Furthermore, a selection of reliable points was applied in order to eliminate experimental points impacted by the slow stabilization of the DSC signal at the beginning of the isotherm (see Supporting Information Figure S4b). After that, the fitting was done using the ≪fit≫ function of the Scilab 6.1.0[39] development tool. The initial time, when the fit with $d\alpha(t)/dt$ is applied, is chosen by default at $t - t_0 = 0$, where t_0 is the beginning of the isothermal crystallization step (Figure 2). The fitting procedure is detailed in the Supporting Information (Figure S4b); it consists of two successive fitting steps of the experimental data divided into two regions.[40] In the first region, only the primary ($\alpha_1(t)$) crystallization is considered, while in the second step, the whole crystallization ($\alpha(t) = w_1{\cdot}\alpha_1(t) + w_2{\cdot}\alpha_2(t)$) is considered for crystallization times up to t_C^{full}.

For each isothermal crystallization curve of PEKK 50/50 between 200 and 290 °C, fitting parameters will be n_1, w_1, K_1, and K_2, while t_0 will be set at the beginning of the isotherm crystallization cycle of the DSC apparatus. Discussion on the choice of t_0 and examples of some fits are reported in the Supporting Information and in Figures S5 and S6. In Figure 5a are presented n_1 and w_1 values deduced from these fits as a function of crystallization temperature, T_C. This evolution will be discussed in the Section 3.2.3 Discussion part.

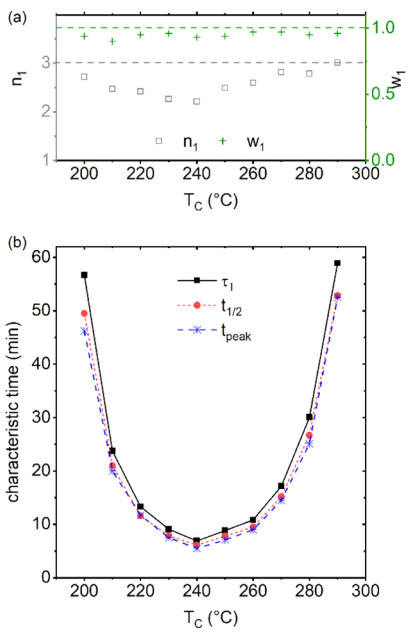

Figure 5. Parameters deduced from the Hillier model as a function of T_C. (a) Avrami exponent n_1 and the weight factor of primary crystallization w_1 and (b) various characteristic times, τ_1, $t_{1/2}$, and t_{peak} (t_{peak} is deduced from the experimental curves in Figure 4).

Various characteristic times, the peak time (t_{peak}), the half-time of crystallization ($t_{1/2}$), and τ_1 are reported in Figure 5b as a function of T_C. Peak time is the time at the maximum crystallization heat flow curve often used in the first studies.[3,8] The half-time of crystallization is the time for which $\alpha(t_{1/2}) = 1/2$, and τ_1 is the characteristic time of the primary crystallization, defined as

$$\alpha_1(t) = 1 - \exp\left(-\left(\frac{t}{\tau_1}\right)^{n_1}\right) \text{ with } \tau_1 = \left(1/K_1\right)^{1/n_1} \quad (14)$$

These three characteristic times evolve in the same way. Their minimum value (~5 min) arrives for T_C around 240 °C, and the three curves present a same U-type shape. The superposition of t_{peak} and $t_{1/2}$ for all T_C is explained by the predominance of primary crystallization. τ_1 is higher than t_{peak} and $t_{1/2}$ because it corresponds to a higher relative crystallinity level of about 0.63 ($\alpha_1(\tau_1) = 1-1/e$) instead of 0.5. The evolution of these three times is discussed in Section 3.2.3.

3.2.2. SAXS–WAXS Experiments. The crystalline structure (nature and amount of crystalline phases) and the crystalline lamella organization during and after isothermal crystallization were studied using, respectively, WAXS and SAXS experiments. To do this, samples were crystallized at various T_C in DSC pans during various crystallization times (t_c) and then quenched at a temperature lower than T_g (Figure 2). Five crystallization temperatures were chosen, 180, 200, 230, 260, and 280 °C, covering the full crystallization temperature range. For 180 and 280 °C, only fully crystallized samples were prepared, whereas for 200, 230, and 260 °C, samples were quenched after various t_c chosen according to the kinetics reported in Figure 4. All these samples are analyzed by SAXS–WAXS and DSC experiments in order to quantify their structure and morphology as well as their melting temperatures and enthalpies.

In Figure 6 are presented WAXS and SAXS spectra (Figure 6a,b) and DSC thermograms (Figure 6c) for samples melt-crystallized at 230 °C during different crystallization times (t_c = 0, 4, 8, 12, 20, and 90 min). The results for the crystallization temperatures of 200 °C and 260 °C are reported in the Supporting Information (Figures S7 and S8).

Before crystallization (t_C = 0 min), PEKK is amorphous, and a broad diffraction halo is observed on the WAXS spectrum, whereas no significant intensity appears on the SAXS spectrum (Figure 6a,b). The DSC trace shows a weak and very broad crystallization exotherm at around 260 °C, followed by a unique and small melting endotherm at 306 °C. All these signals evolve as the crystallization time progresses.

Sharp Bragg peaks appear at q = 1.31, 1.61, and 2.01 $Å^{-1}$, and they are associated with the crystalline form I (Table S2 in the Supporting Information). Their indexation in the orthorhombic crystal cell of form I is reported Figure 6a.[15] The small Bragg peaks at 1.41 and 1.49 $Å^{-1}$, attributed to form III, appear for the longest crystallization times. When t_C increases, the position of these Bragg peaks remains constant and their intensities increase, leading to an increase of the weight crystallinity χ_c^w. The evolution of χ_c^w is reported in Figure 7a.

The correlation peak observed on SAXS spectra (Figure 6b) is characteristic of the periodic organization of the crystalline lamellae. Their integrated intensity is quantified by the invariant, Inv, defined in the Experimental Section (Section 2.3). This integrated intensity increases significantly with t_C as the total crystallinity increases. From these SAXS spectra, we have calculated the correlation function of the electronic density K(z), reported in Figure 6d. The thickness of the crystalline lamellae L_C and their long period L_P are deduced from these curves [see the Experimental Section (Section 2.3) and Figure S2]. L_P and L_C deduced from these experiments correspond to average values of the respective distributions of L_P and L_C. The decrease of L_P and L_C observed when the crystallization progresses (Figure 7d,e) corresponds to a shift of these respective distributions toward lower values. Thicker lamellae would be formed at the beginning of the

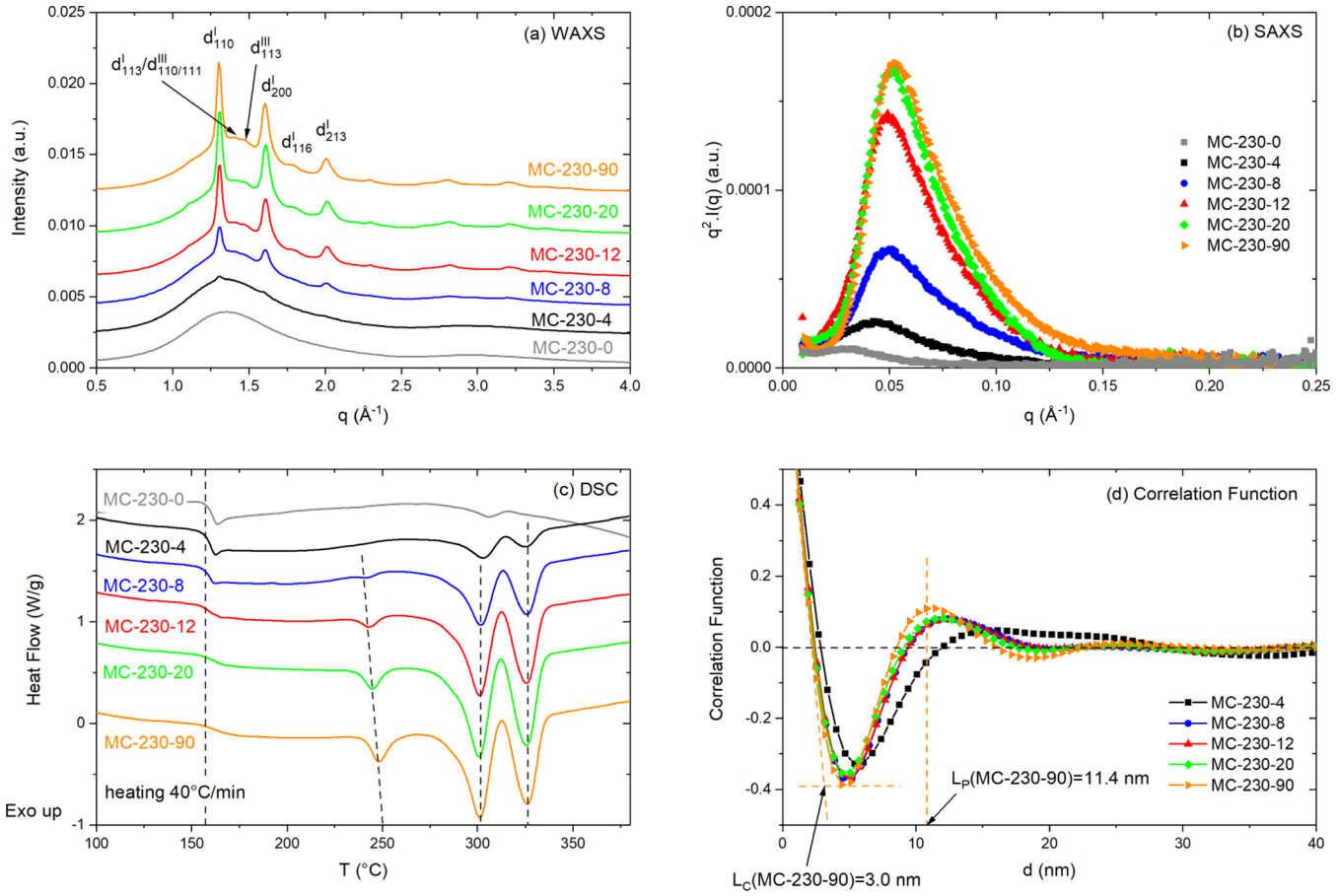

Figure 6. PEKK 50/50 crystallized at 230 °C during 0, 4, 8, 12, 20, and 90 min analyzed by (a) WAXS, (b) SAXS, and (c) DSC experiments. (d) Correlation function deduced from SAXS.

crystallization, and thinner lamellae would be formed at the end of the crystallization. As detailed in the Experimental Section and in the Supporting Information, the linear crystallinity χ_C^L can be calculated using the correlation function $K(z)$ from two different ways. The value reported in Figure 7d is deduced from the expression (7). χ_C^L reaches its final value from the very beginning of crystallization (Figure 7d). This observation and the comparison with the evolution of the weight crystallinity will be discussed later.

The first heating DSC curves after the various crystallization times are reported in Figure 6c. For all these samples, a glass-transition temperature, T_g, is observed at around 160 °C and then a small endothermic peak at T_m^{Low} around 250 °C, followed by two large endothermic peaks at around 301 °C (T_{m2}) and 326 °C (T_{m3}).

A slight increase of the glass-transition temperature, T_g, is observed from 158.9 to 161.6 °C, associated with a significant decrease of the ΔC_p, from 0.293 to 0.130 J/g·°C, when the crystallization progresses from t_c = 0 to 90 min. These evolutions reflect a stiffening of the amorphous phase as well as a decrease of its amount during crystallization.[19,41]

The temperature of the small endothermic peak, T_m^{Low}, increases from 242 to 248 °C when t_c increases from 4 to 90 min. According to a previous study, this endotherm is associated with the melting of secondary fringed micellar crystals formed in the constrained amorphous phase.[19] This evolution with the crystallization time was already observed and reported on PEEK[28] and PEKK[29] samples.

The main endothermic event, between 275 and 340 °C, is constituted of two endothermic peaks localized, respectively, at T_{m2} and T_{m3}. When the crystallization time increases from 0 to 90 min, no significant evolution of T_{m2} and T_{m3} is observed, while an obvious increase of the enthalpy, ΔH_m, is measured associated with the increase in crystallinity (Figure 7b).

All the quantitative data deduced from WAXS, SAXS, and DSC experiments along the crystallization process at 200, 230, and 260 °C are gathered in Figure 7. This Figure 7 is discussed in Section 3.2.3.

3.2.3. Discussion on the Crystallization Kinetics. 3.2.3.1. Parameters Deduced from the Hillier Model. We used the Hillier model with adjustable n_1 to fit our crystallization curves (see section 3.2.1). The parameters deduced from the fitting of the experimental crystallization curves are the weight factor of primary crystallization w_1, the Avrami exponent n_1, and the two crystallization rate constants K_1 and K_2. Using these parameters, the relative crystallinity, $\alpha(t)$, was calculated after integration of eq 13 and the half-time of crystallization $t_{1/2}$ was deduced.

The evolution of w_1 and n_1 as a function of the crystallization temperature T_C is reported in Figure 5a. w_1 remains close to 1 ($w_1 = 0.95 \pm 0.03$) in the whole range of T_C, meaning that the primary crystallization is predominant for this PEKK 50/50 copolymer, independent of T_C. In this T_C range, n_1 evolves between 2.2 and 3.0 with its lowest value for T_C = 240 °C. To the best of our knowledge, this is the first work reporting w_1 and n_1 values for PEKK 50/50. Choupin et al.[17] have used the

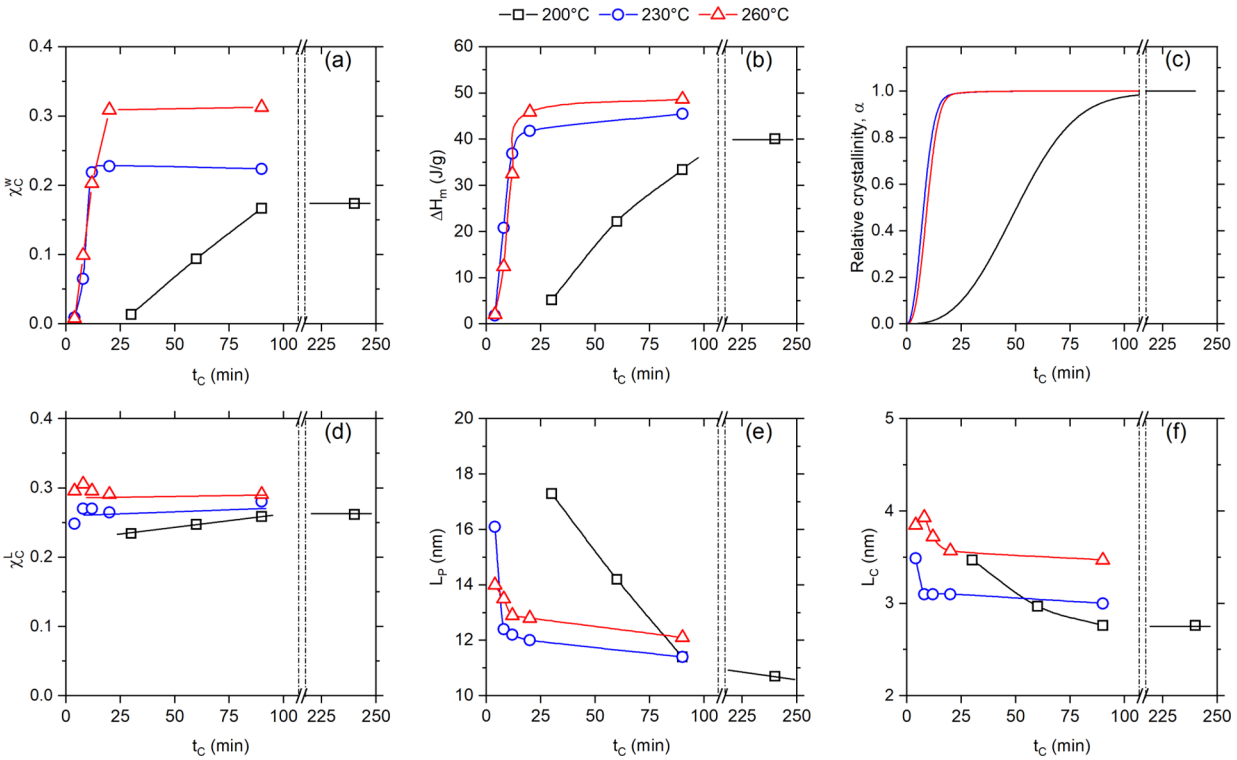

Figure 7. Evolution of structural parameters as a function of the crystallization time t_c during isothermal crystallization: (a) weight crystallinity χ_c^w, (b) melting enthalpy ΔH_m, (c) relative crystallinity deduced from the Hillier model $\alpha(t)$, (d) linear crystallinity χ_c^L, (e) crystalline lamella periodicity L_p, and (f) crystalline lamella thickness L_c.

same Hillier model and fitting procedure, although fixing the exponents $n_1 = 3$ and $n_2 = 1$, to study the crystallization kinetics of PEKK 70/30 and PEKK 60/40. They found a relatively high and constant value of w_1 ($w_1 = 0.8$) between 250 and 300 °C for PEKK 70/30, while for PEKK 60/40, the w_1 parameter decreases from 0.65 to 0.4 when T_C increases from 200 °C to 270 °C.[17] On the other hand, Chelaghma et al. applied the generalized Hillier model (with $n_1 = 3$ and $n_2 = 2.7$) to study the crystallization kinetics of PEKK 70/30. They found decreasing w_1 values from 0.95 to 0.55 for T_C between 270 and 290 °C.[18] These various data show the strong interdependence of w_1, n_1, and n_2 values and the complexity of the crystallization process for PEKK copolymers.

It is worth to note that Piorkowska et al.[34] have questioned the physical meaning of the parameters K and n extracted from the fitting of various crystallization models. According to these authors, crystallization models are based on strong assumptions which, generally, are not experimentally satisfied as for instance when considering spherulites as being the growing ≪crystalline volume≫ with a constant growth rate and constant density[31,34] or when using the weight crystallinity (that is, deduced from a DSC experiment, as done here) with model predictions on the evolution of a crystalline volume.

We agree with Piorkowska et al.,[34] and we are aware of these weaknesses and drawbacks. However, we consider the parameters extracted from these fittings (n_1, w_1, and K_1) as useful adjustable parameters for the description of the crystallization process even if their physical meaning requires further clarification. What however comes clearly out of our study is that PEKK 50/50 exhibits quite simple crystallization kinetics (essentially primary) as compared to other PEKKs. We used these parameters to calculate the crystallization times, $t_{1/2}$ and τ_1 (eq 14), the fraction of primary crystallization, and the total crystallization enthalpy.

The crystallization times, $t_{1/2}$, t_{peak}, and τ_1, deduced from our analysis are reported in Figure 5b. The three curves exhibit a same U-shape with a minimum for $T_C \sim 240$ °C. The driving force for crystallization increases with the undercooling ($T_m - T_C$), and sufficient polymer chain mobility is necessary for crystallization.[33] Near the melting point, the driving force is very low, while the chain mobility is high, and inversely at a low temperature, near T_g, the driving force for crystallization is maximum and the chain mobility is very low. These two opposite effects explain the U-shape of the curve.[33] t_{peak} and $t_{1/2}$ have very close values explained by the predominance of primary crystallization. τ_1 is calculated from K_1 and n_1 (eq 14) and corresponds to a primary crystallization level of 0.63 ($\alpha_1(\tau) = 1-1/e$). As primary crystallization is dominant in our case, τ_1 appears slightly higher than $t_{1/2}$ in Figure 5b. The minimum value of t_{peak}, around 5 min, is intermediate between values recently measured for PEKK 60/40 ($t_{peak} \sim 7$ min)[17] and PEKK 70/30 ($t_{peak} \sim 1$ min).[17,18] For PEKK copolymers with a high T/I ratio, Gardner et al.[3] observed that the crystallization rates increase in the order (60/40) < (70/30) ≈ (80/20) < (90/10) and that the homopolymer (50/50) has a specific behavior with a crystallization rate intermediate between that of (60/40) and that of (70/30). Our study confirms this observation that highlights the specificity of the PEKK 50/50 with its regular TI diad repetition.

3.2.3.2. Structural Parameters from SAXS–WAXS Experiments during Isothermal Crystallization. The evolution of the structural parameters during isothermal crystallization at various T_C are reported in Figure 7. The increase of the weight crystallinity (WAXS) of the melting enthalpy (DSC) and of the relative crystallinity $\alpha(t)$ during crystallization at various

T_C are reported, respectively, in Figure 7a–c. The shape of these curves, reflecting the crystallization rates, is in line with the characteristic times reported in Figure 5b, that is, the half-time of crystallization around few minutes for T_C = 230 and 260 °C and around 60 min for T_C = 200 °C. The crystallinity reached at the end of crystallization (long times) increases with T_C (Figure 7a). On the other hand, the linear crystallinity (Figure 7d), which corresponds to the crystalline fraction inside stacks of crystalline lamellae, does not show the same kinetics. The final value of χ_c^L (between 0.25 and 0.30) seems to be reached from the first minutes of crystallization regardless of T_C. Stacks of crystalline lamellae form at the beginning of the crystallization process. These stacks are composed of crystalline lamellae of thickness L_C organized periodically (period L_P) with the amorphous layer (thickness L_a). The stacks are embedded in the amorphous phase at the beginning of the crystallization process, and they constitute the core of the spherulites.

The values of L_P and L_C deduced from SAXS measurements correspond to the mean value of the distribution of distances in the material. These average values of L_P and L_C decrease when the crystallization time increases (Figure 7e,f). These decreases correspond to a modification of the distribution and to the appearance of thinner crystalline lamellae. A similar evolution was already observed in PEEK[42] and attributed to the crystallization of thinner crystals in amorphous pockets between thick primary lamellae during secondary crystallization.[43] A decrease of L_P and L_C was also reported for PEKK (50/50) crystallized between 240 and 280 °C.[44] As indicated by our results, secondary crystallization is not significant for PEKK 50/50, so we conclude that during primary crystallization, the thickness and the periodicity of the crystalline lamellae decrease as the lateral growth of the crystalline lamella progresses.

A similar evolution of L_C and L_P with the crystallization time was reported by Wang et al.[44] Although we measure the same L_P as Wang et al., around 12 nm, we conclude on very different L_C values: $L_C \sim 10$ nm in ref 44 and $L_C \sim 3$ nm in the present study. Indeed, from the correlation function deduced from SAXS analysis, the choice for the various thicknesses, L_C and L_a, is not unique and we do not make the same choice as Wang et al. Our choice, based in particular on the comparison between weight and linear crystallinities, is discussed in the Supporting Information.

Finally, it is interesting to notice that during the crystallization process, the position of the Bragg peaks does not change when t_C increases, whatever the crystallization temperature is, 200, 230, or 260 °C (Figures S7, 6a, and S8, respectively). Thus, we can conclude that the density of the crystalline lamellae does not evolve during crystallization. Hsiao et al. reported a similar observation for isothermal crystallization of PEKK 50/50 at 200 °C.[16]

3.3. Structure and Morphology of Fully Crystallized Samples. In this section, we study the crystalline structure state after full crystallization for T_C ranging from 180 to 280 °C. The SAXS and WAXS spectra are reported in Figure 8. The position of the correlation peak observed on the SAXS spectra (Figure 8a) changes slightly with T_C reflecting a change in L_P. A significant evolution in the shape of this peak should be noted, and the full width at half-maximum (fwhm) decreases when T_C increases, showing an improvement in the crystalline lamella stacking. An additional peak at q around 0.2 Å^{-1} appears for T_C = 280 °C. The increase of the crystallinity is obvious in Figure 8b, and Bragg peaks are higher and thinner for the highest T_C. As already observed,[16] the crystalline form II only appears for the lowest T_C, and a small peak is observed at q around 1.12 Å^{-1}. Bragg peaks of form III, located around 1.43 and 1.49 Å^{-1}, are well defined for T_C higher than 260 °C. A thinning of the (110) Bragg peak is observed, reflecting an increase of the crystal correlation length along D_{110}.

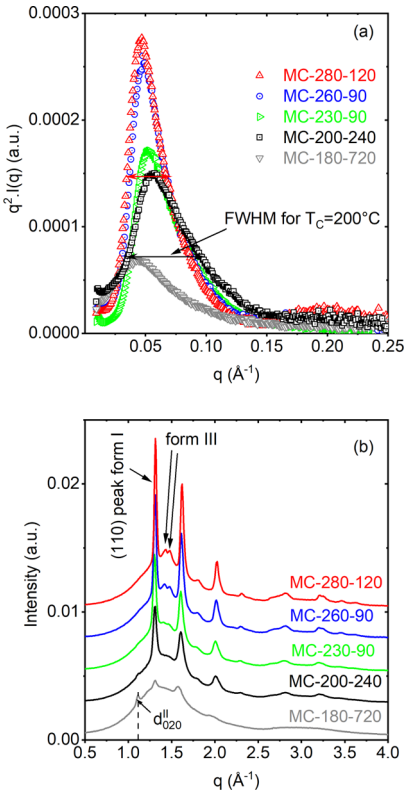

Figure 8. Crystallization obtained for various T_C and after long t_C: (a) SAXS spectra highlighting the decrease of correlation peak width (fwhm) at high T_C and (b) WAXS spectra showing the existence of form II for the lowest T_C and the appearance of form III at high T_C.

Characteristic structural parameters are gathered in Figure 9. The linear and weight crystallinities deduced from SAXS–WAXS experiments and the crystallization and melting enthalpies deduced from DSC increase with T_C (Figure 9a).

It is interesting to note that the curves reported in Figure 9 do not exhibit any symmetry, unlike what is obtained for the half-time of crystallization, which exhibits a U-type curve as a function T_C (Figure 5b). The crystallization is slow, with $t_{1/2}$ around 1h00, for T_C = 200 and 290 °C, and it is faster, with a $t_{1/2}$ around 5 min, for T_C = 240 °C. Although the crystallization kinetics appears similar at low and high temperatures, morphologies and crystallinities are different. As reported in Figure 9a, the weight crystallinity χ_c^w is low (<10%) after crystallization at low temperatures and reaches 30% for crystallization at temperatures higher than 260 °C. The crystallization and melting enthalpies (Figure 9a), ΔH_C and ΔH_m, respectively, evolve in the same way as χ_c^w. On the other hand, the linear crystallinity χ_c^L shows only a slight dependence on T_C evolving between 24 and 29% for T_C ranging from 180 to 280 °C. It seems that the lateral growth of the crystalline lamellae is not efficient at a low T_C, 180 °C, resulting in a partially crystallized sample even after 12 h (t_C = 720 min) of isothermal crystallization (gray area in Figure 9).

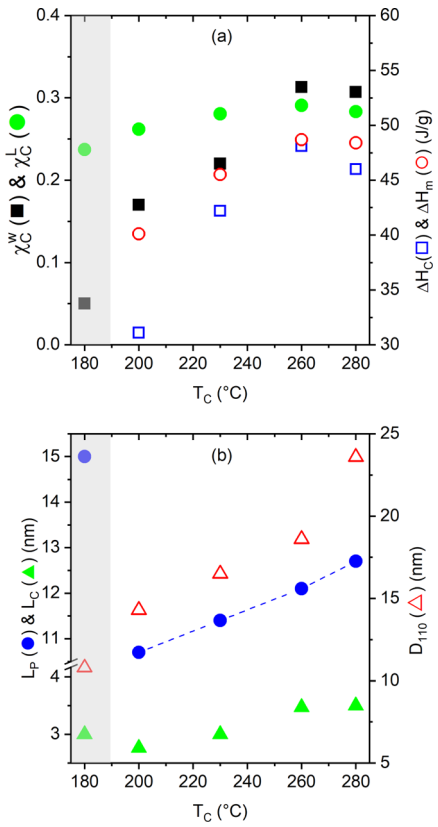

Figure 9. Evolution of structural parameters with T_C: (a) total weight and linear crystallinity, χ_c^w and χ_c^L, and crystallization and melting enthalpy, ΔH_C and ΔH_m and (b) crystalline lamella periodicity L_P (the dotted line is a guide for the eye), thickness L_C, and lateral extension D_{110}. The gray area highlights the crystallization temperature range in which only partially crystallized samples are obtained.

The thickness (L_C) and the lateral extension of the crystalline lamellae (D_{110}) increase simultaneously with T_C, as well as their periodicity L_P (Figure 9b). An increase of L_C, from 2.7 to 3.5 nm, and of L_P, from 10.7 to 12.7 nm, when T_C increases from 200 to 280 °C is observed. The increase of L_C when decreasing undercooling is experimentally observed for many polymers, see, for instance, refs 33 and 44−46, and also theoretically predicted.[33] The correlation length D_{110}, perpendicular to the chain direction, increases from 11 to 24 nm when T_C increases from 180 to 280 °C, indicating a perfection of the crystalline order in the crystalline lamellae. The same kind of evolution was already reported for polyethylene and in polypropylene by Schultz.[33] At the same time, the narrowing of the SAXS signal (reduction of the fwhm by a factor of 2, see Figure 8a) indicates a perfection of the stacking of the crystalline lamellae. It corresponds to a narrower distribution of their thickness and periodicity. The higher mobility of the chains at high temperatures (i.e., lower undercooling) improves the crystal perfection.

Finally, it is interesting to observe that after crystallization from the melt, form II is only a very minor phase, whereas it is the main phase obtained after the synthesis. Indeed, as reported by Hsiao et al.,[16] the crystalline forms I and III are observed regardless of the crystallization temperature T_C, while form II appears as very minor only for low T_C.

4. IS PEKK 50/50 A GOOD CANDIDATE FOR HT-LS?

The thermal and crystallization behavior of PEKK 50/50 seems to meet the requirements for use in additive manufacturing and more specifically in LS:

- The crystallization kinetics is slow ($t_{1/2}$ > 20 min for T_C > 270 °C), similar to the one reported for PEKK 60/40[17,47] and clearly slower than that of PEEK.[43,48]
- The reached crystallinity is high, around 30 wt %, higher than that of PEKK 60/40[19,29,47,49] or PEEK.[48,50]
- The crystallization kinetics, almost only primary, is very simple as compared to those of other PEKK or PEEK.[17,18,42,43]

Although the as-received polymer exhibits a complex thermal profile upon heating (Figure 3a), adequate thermal treatment (annealing) makes this profile much simpler. See, for instance, the DSC trace of the powder annealed 90 min at 295 °C (Figure 10a) which does not exhibit any significant endothermic or exothermic peaks below 300 °C. Therefore, no partial melting or crystallization of the powder grains is expected at T < 300 °C.

During the HT-LS process, the polymer powder is introduced layer upon layer on the building platform of the LS equipment, which is maintained at a temperature of T_{bp} and

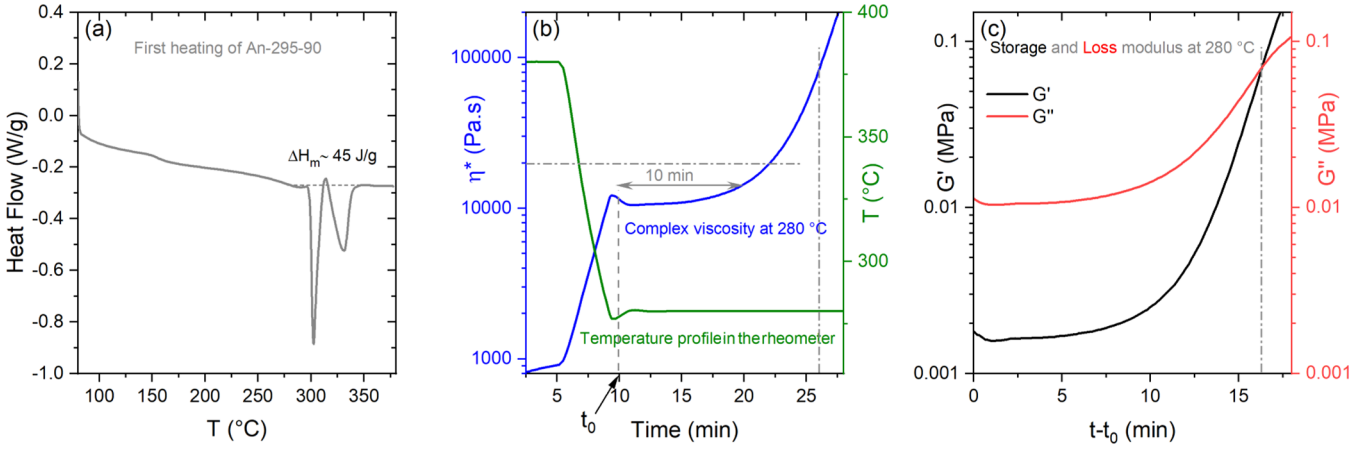

Figure 10. : Thermal and rheological measurements on PEKK 50/50: (a) DSC first heating curve of a sample annealed at 295 °C for 90 min (An-295-90), (b) complex viscosity during the temperature ramp in a parallel plate rheometer (5 min at 380 °C, 5 min from 380 to 280 °C, and then constant at T_C = 280 °C, t_0 is the starting time of this isothermal step), and (c) storage and loss modulus during the isotherm at 280 °C.

lowers down by a step of ∼100 μm before the introduction of a new polymer layer. The surface of the powder bed is heated at T_{bed} by infrared heaters positioned above the powder bed. Once T_{bed} is reached, the laser beam scans the surface and selectively melts the powder at the regions where the part slice has to be formed. For semicrystalline polymers, T_{bed} is set very near to the onset of the melting peak, while T_{bp} is usually 15−30 °C below T_{bed}.[47,51,52] These conditions allow process optimization and improved part quality by reducing thermal gradients, the crystallization rate, shrinkage, and risks of curling and warping. For a more detailed description of LS equipment, process conditions, and T_{bed} and T_{bp} choice, the reader is referred to refs 47 and 51−53.

Note that this is a very simplified description of the LS process because it does not consider the local temperature variations due to the coating of each new powder layer which arrives at a temperature lower than T_{bed}. A more complete description of the HT-LS process was published recently by Chen et al. using a PEEK powder.[53] For polymers exhibiting fast crystallization, such as PEEK, local temperature variations may have a strong impact on the crystallization of the molten powder during the LS process. This imposes a strict selection of the sintering window (temperature window between the onset of the melting peak during a heating scan and the onset of the crystallization peak during a cooling scan) and of the contribution of non-isothermal crystallization around T_{bp}.[53] However, for a slowly crystallized polymer, such as PEKK 50/50, such temperature variations are expected to have less impact on the crystallization.

During the LS process, the unscanned powder experiences temperatures close to T_{bp} for quite long periods of time. During this period, it should not melt or undesirably sinter. The melting profile of PEKK 50/50 shown in Figure 10a seems to satisfy this requirement.

Considering the thermal properties of PEKK 50/50 and inspired form the work of Benedetti et al.[47] on PEKK 60/40, another member of the PEKK family provided by Arkema as Kepstan 6002,[9] we can estimate T_{bed} to be of the order of 295−300 °C and T_{bp} ∼ 280 °C. It is interesting to note that at 280 °C, the PEKK 50/50 crystallization rate remains slow, $t_{1/2}$ ∼ 20 min, indicating a slow evolution of the rheological properties of the molten powder at this temperature, a prerequisite for good coalescence and consolidation.[47,54]

Figure 10b shows the evolution of the complex viscosity of PEKK 50/50 at 280 °C after melting at 380 °C. The viscosity remains almost constant for a time of ∼10 min, during which the grains can coalesce. Beyond this time, the viscosity increases as the crystallization proceeds. The melt viscosity at 280 °C increases by a factor of 2 after 12 min (Figure 10b), while the gel point ($G' = G''$) is reached after 16 min (Figure 10c). At this time, the relative crystallinity is around 0.15; thus, the weight crystallinity χ_c^w is around 4%.

Finally, the annealed PEKK 50/50 presents a high enthalpy of melting at this temperature range, ΔH_m ∼45 J/g (Figure 10a), higher than that of PEKK 60/40[19,29,47,49] or PEEK.[50] A high ΔH_m is of importance for preventing heat transfer to the powder particles adjacent to those intended to be fused by the laser.[51]

5. CONCLUSIONS

We studied the isothermal melt crystallization of PEKK 50/50, the kinetics, and the crystalline structure and morphologies for various crystallization temperatures, T_C. As-synthesized PEKK 50/50 crystallizes in form II. After annealing, a mixture of form I and form II is obtained depending on the annealing temperature. Endothermic events measured with the as-synthesized powder occur between 250 and 350 °C, with three endothermic peaks at around 270, 300, and 330 °C.

The melt crystallization isotherms were studied over a wide range of T_C from 200 to 290 °C and analyzed with a Hillier model. Primary crystallization dominates ($w_1 > 0.9$) whatever T_c, and an Avrami exponent, n_1, between 2.2 and 3, was deduced. The half-time of crystallization, $t_{1/2}$, was measured between 6 and 60 min; the minimum value is observed for T_C = 240 °C, and the maximum one is observed for T_C = 200 and 290 °C.

At the beginning of the crystallization process, stacks of periodic crystalline and amorphous lamellae are created, with crystalline lamella thickness, L_C, and periodicity, L_P. In these stacks, the linear crystallinity reaches quickly its final value. Then, the growth of crystalline lamellae continues laterally, contributing to the gradual weight crystallinity increase. During this time, the crystalline lamellae grow thinner and thinner, leading to the decrease of their average thickness, L_C, and average periodicity, L_P, as shown by SAXS. From WAXS experiments, we deduce that the density of the crystalline lamellae, ρ_C, remains constant during the crystallization process.

Although the crystallization kinetics at 200 and 280 °C appear similar (same $t_{1/2}$), the final crystalline states reached are different. Indeed, the weight crystallinity, the crystalline perfection inside the crystalline lamellae, and the perfection of the crystalline lamella stacking increase with T_C. This perfection is reached, thanks to the high mobility of the PEKK chains at high T_C.

The moderate crystallization rate and the rheological behavior observed at 280 °C are encouraging elements for future use of PEKK 50/50 in HT-LS.

■ ASSOCIATED CONTENT

Supporting Information

The Supporting Information is available free of charge at https://pubs.acs.org/doi/10.1021/acsapm.2c00096.

Details on the diad description in PEKK T/I ≤ 50/50; list of the samples along with the experimental conditions; details on the correlation function analysis; details on the calculated interplanar distances; details on the treatment of the DSC crystallization isotherm; SAXS−WAXS and DSC results for T_C = 200 °C and T_C = 260 °C (PDF)

■ AUTHOR INFORMATION

Corresponding Author

Sylvie Tencé-Girault − *Laboratoire PIMM, Arts et Metiers Institute of Technology, CNRS, Cnam, HESAM Universite, Paris 75013, France; Arkema, CERDATO, Route du Rilsan, Serquigny 27470, France;* orcid.org/0000-0001-5090-2334; Email: sylvie.girault@ensam.eu

Authors

Alexis Cherri − *Laboratoire PIMM, Arts et Metiers Institute of Technology, CNRS, Cnam, HESAM Universite, Paris 75013, France*

Ilias Iliopoulos − *Laboratoire PIMM, Arts et Metiers Institute of Technology, CNRS, Cnam, HESAM Universite, Paris 75013, France*
Gilles Régnier − *Laboratoire PIMM, Arts et Metiers Institute of Technology, CNRS, Cnam, HESAM Universite, Paris 75013, France*
Benoit Brulé − *Arkema, CERDATO, Route du Rilsan, Serquigny 27470, France*
Guillaume Lé − *Arkema, CERDATO, Route du Rilsan, Serquigny 27470, France*

Complete contact information is available at: https://pubs.acs.org/10.1021/acsapm.2c00096

Notes

The authors declare no competing financial interest.

■ ACKNOWLEDGMENTS

This work is dedicated to memory of Christian Collette, CTO of Arkema, who passed away in April 2021. His scientific intelligence, open mind, and open innovation approach have been a source of inspiration for his colleagues and in particular for the authors of the present work. Our colleagues from PIMM, Lauriane Truffault, Alain Guinault, and Jorge Peixinho, are warmly thanked for their valuable advice and technical assistance during the DSC and rheology experiments. Sylvie Lebreton and François Bargain are thanked for their warm welcome during SAXS−WAXS experiments at the LEM laboratory, Arkema, Serquigny. This research was carried out within the framework of the Industrial Chair Arkema (Arkema/CNRS-ENSAM-Cnam, Arkema no AC-2018-413, CNRS no 183697); authors concerned: all.

■ REFERENCES

(1) Veazey, D.; Hsu, T.; Gomez, E. D. Next generation high-performance carbon fiber thermoplastic composites based on polyaryletherketones. *J. Appl. Polym. Sci.* **2016**, *134*, 44441.
(2) Pérez-Martín, H.; Mackenzie, P.; Baidak, A.; Ó Brádaigh, C. M.; Ray, D. Crystallinity studies of PEKK and carbon fibre/PEKK composites: A review. *Composites, Part B* **2021**, *223*, 109127.
(3) Gardner, K. H.; Hsiao, B. S.; Matheson, R. R.; Wood, B. A. Structure, crystallization and morphology of poly (aryl ether ketone ketone). *Polymer* **1992**, *33*, 2483−2495.
(4) Blundell, D. J.; Newton, A. B. Variations in the crystal lattice of PEEK and related para-substituted aromatic polymers: 2. Effect of sequence and proportion of ether and ketone links. *Polymer* **1991**, *32*, 308−313.
(5) Zolotukhin, M. G.; Rueda, D. R.; Balta Calleja, F. J.; Cagiao, M. E.; Bruix, M.; Sedova, E. A.; Gileva, N. G. Aromatic polymers obtained by precipitation polycondensation: 4. Synthesis of poly-(ether ketone ketone)s. *Polymer* **1997**, *38*, 1471−1476.
(6) Gardner, K. H.; Hsiao, B. S.; Faron, K. L. Polymorphism in poly(aryl ether ketone)s. *Polymer* **1994**, *35*, 2290−2295.
(7) Le, G., Jouanneau, J., Clair, N., Process for producing polyether ketone ketone. European Patent 3 438 085 A1, 02 06 2019.
(8) Hsiao, B. S.; Gardner, K. H.; Cheng, S. Z. D. Crystallization of poly(aryl ether ketone ketone) copolymers containing terephthalate/isophthalate moieties. *J. Polym. Sci., Part B: Polym. Phys.* **1994**, *32*, 2585−2594.
(9) Kepstan® PEKK Resins for Extremely Demanding Applications [Online]. Available. https://www.extrememateriels-arkema.com/en/product-families/kepstan-pekk-polymer-range [accessed Aug 11, 2021].
(10) Geslin, A.; Paul, C.; Bussi, P.; Barsotti, R.; Hollahan, J.; Calvin, M. PEKK Poly Ether Ketone Ketone for High Temperature High Pressure Oil & Gas Conditions. *Offshore Technology Conference*; OnePetro: Houston, Texas, August 2021.
(11) Avenet, J.; Levy, A.; Bailleul, J.-L.; Le Corre, S.; Delmas, J. Adhesion of high performance thermoplastic composites: Development of a bench and procedure for kinetics identification. *Composites, Part A* **2020**, *138*, 106054.
(12) Benedetti, L.; Brulé, B.; Decreamer, N.; Evans, K. E.; Ghita, O. Shrinkage behaviour of semi-crystalline polymers in laser sintering: PEKK and PA12. *Mater. Des.* **2019**, *181*, 107906.
(13) Peyre, P.; Rouchausse, Y.; Defauchy, D.; Régnier, G. Experimental and numerical analysis of the selective laser sintering (SLS) of PA12 and PEKK semi-crystalline polymers. *J. Mater. Process. Technol.* **2015**, *225*, 326−336.
(14) Lepoivre, A.; Levy, A.; Boyard, N.; Gaudefroy, V.; Sobotka, V. Coalescence in fused filament fabrication process: Thermo-dependent characterization of high-performance polymer properties. *Polym. Test.* **2021**, *98*, 107096.
(15) Ho, R.-M.; Cheng, S. Z. D.; Hsiao, B. S.; Gardner, K. H. Crystal Morphology and Phase Identification in Poly(aryl ether ketone)s and Their Copolymers. 3. Polymorphism in a Polymer Containing Alternated Terephthalic Acid and Isophthalic Acid Isomers. *Macromolecules* **1995**, *28*, 1938−1945.
(16) Hsiao, B. S.; Ho, R.-M.; Cheng, S. Z. D. Time-resolved synchrotron X-ray study of crystalline phase transition in poly(aryl ether ketone ketone) containing alternated terephthalic/isophthalic moieties. *J. Polym. Sci., Part B: Polym. Phys.* **1995**, *33*, 2439−2447.
(17) Choupin, T.; Fayolle, B.; Régnier, G.; Paris, C.; Cinquin, J.; Brulé, B. A more reliable DSC-based methodology to study crystallization kinetics: Application to poly(ether ketone ketone) (PEKK) copolymers. *Polymer* **2018**, *155*, 109−115.
(18) Chelaghma, S. A.; De Almeida, O.; Margueres, P.; Passieux, J. C.; Perie, J. N.; Vinet, A.; Reine, B. Identification of isothermal crystallization kinetics of poly(ether-ketone-ketone) based on spherulite growth measurements and enthalpic data. *Polym. Cryst.* **2020**, *3*, 10141.
(19) Tencé-Girault, S.; Quibel, J.; Cherri, A.; Roland, S.; Fayolle, B.; Bizet, S.; Iliopoulos, I. Quantitative Structural Study of Cold-Crystallized PEKK. *ACS Appl. Polym. Mater.* **2021**, *3*, 1795−1808.
(20) Lorenzo, A. T.; Arnal, M. L.; Albuerne, J.; Müller, A. J. DSC isothermal polymer crystallization kinetics measurements and the use of the Avrami equation to fit the data: Guidelines to avoid common problems. *Polym. Test.* **2007**, *26*, 222−231.
(21) Foxtrot software can be obtained by sending a mail to foxtrot@xenocs.com. Software is free for non-profit usage, directly usable with Nexus and ESRF 2D data format.
(22) Wojdyr, M. Fityk: a general-purpose peak fitting program. *J. Appl. Crystallogr.* **2010**, *43*, 1126−1128.
(23) Klug, M. J., Alexander, L. E., *X-ray Diffraction Procedures: for Polycrystalline and Amorphous Materials*, 2, New York: Wiley-Interscience, 1974.
(24) Bargain, F.; Thuau, D.; Panine, P.; Hadziioannou, G.; Domingues Dos Santos, F.; Tencé-Girault, S. Thermal behavior of poly(VDF-ter-TrFE-ter-CTFE) copolymers: Influence of CTFE termonomer on the crystal-crystal transitions. *Polymer* **2019**, *161*, 64−77.
(25) Strobl, G. R.; Schneider, M. Direct evaluation of the electron density correlation function of partially crystalline polymers. *J. Polym. Sci., Polym. Phys. Ed.* **1980**, *18*, 1343−1359.
(26) Santa Cruz, C.; Stribeck, N.; Zachmann, H. G.; Balta Calleja, F. J. Novel aspects in the structure of poly(ethylene terephthalate) as revealed by means of small angle x-ray scattering. *Macromolecules* **1991**, *24*, 5980−5990.
(27) XSACT: X-ray Scattering Analysis and Calculation Tool. SAXS &WAXS Data Analysis Software-Available online : http://www.xenocs.com/products/software, [Online] [Accessed Feb 22, 2022].
(28) Marand, H.; Alizadeh, A.; Farmer, R.; Desai, R.; Velikov, V. Influence of Structural and Topological Constraints on the Crystallization and Melting Behavior of Polymers. 2. Poly(arylene ether ether ketone). *Macromolecules* **2000**, *33*, 3392−3403.

(29) Cortès, L. Q.; Caussé, N.; Dantras, E.; Lonjon, A.; Lacabanne, C. Morphology and dynamical mechanical properties of poly ether ketone ketone (PEKK) with meta phenyl links. *J. Appl. Polym. Sci.* **2016**, *133*, 43396.
(30) Hoffman, J. D.; Lauritzen, J. I. Crystallization of Bulk Polymers With Chain Folding: Theory of Growth of Lamellar Spherulites. *J. Res. Natl. Bur. Stand., Sect. A* **1961**, *65*, 297−336.
(31) Hillier, I. H. Modified Avrami Equation for the Bulk Crystallization Kinetics of Spherulitic Polymers. *J. Polym. Sci., Part A: Gen. Pap.* **1965**, *3*, 3067−3078.
(32) Billon, N.; Escleine, J. M.; Haudin, J. M. Isothermal crystallization kinetics in a limited volume. A geometrical approach based on Evans' theory. *Colloid Polym. Sci.* **1989**, *267*, 668−680.
(33) Schultz, J. M. *Polymer Crystallization: The Development of Crystalline Order in Thermoplastic Polymers*; American Chemical Society: Université du Michigan, 2001.
(34) Piorkowska, E.; Galeski, A.; Haudin, J.-M. Critical assessment of overall crystallization kinetics theories and predictions. *Prog. Polym. Sci.* **2006**, *31*, 549−575.
(35) Velisaris, C. N.; Seferis, J. C. Crystallization Kinetics of Polyetheretherketone (PEEK) Matrices. *Polym. Eng. Sci.* **1986**, *26*, 1574−1581.
(36) Peterlin, A. Secondary Crystallization and Annealing of Polyethylene. *J. Appl. Phys.* **1964**, *35*, 75−81.
(37) Price, F. P. A Phenomenological Theory of Spherulitic Crystallization: Primary and Secondary Crystallization Processes. *J. Polym. Sci., Part A: Gen. Pap.* **1965**, *3*, 3079−3086.
(38) Hsiao, B. S.; Chang, I. Y.; Sauer, B. B. Isothermal crystallization kinetics of poly(ether ketone ketone) and its carbon-fibre-reinforced composites. *Polymer* **1991**, *32*, 2799−2805.
(39) Scilab [Online]. Available: https://www.scilab.org/about. [Accessed 11 01, 2022].
(40) Perez-Cardenas, F. C.; Del Castillo, L. F.; Vera-Graziano, R. Modified Avrami Expression for Polymer Crystallization Kinetics. *J. Appl. Polym. Sci.* **1991**, *43*, 779−782.
(41) Krishnaswamy, R. K.; Kalika, D. S. Glass transition characteristics of poly(aryl ether ketone ketone) and its copolymers. *Polymer* **1996**, *37*, 1915−1923.
(42) Verma, R.; Marand, H.; Hsiao, B. Morphological Changes during Secondary Crystallization and Subsequent Melting in Poly(ether ether ketone) as Studied by Real Time Small Angle X-ray Scattering. *Macromolecules* **1996**, *29*, 7767−7775.
(43) Seo, J.; Gohn, A. M.; Dubin, O.; Takahashi, H.; Hasegawa, H.; Sato, R.; Rhoades, A. M.; Schaake, R. P.; Colby, R. H. Isothermal crystallization of poly(ether ether ketone) with different molecular weights over a wide temperature range. *Polym. Cryst.* **2019**, *2*, 10055.
(44) Wang, W.; Schultz, J. M.; Hsiao, B. S. Anomalous two-stage spherulite growth in poly(aryl ether ketones) during isothermal crystallization. *J. Polym. Sci., Part B: Polym. Phys.* **1996**, *34*, 3095−3105.
(45) Strobl, G. Colloquium: Laws controlling crystallization and melting in bulk polymers. *Rev. Mod. Phys.* **2009**, *81*, 1287−1300.
(46) Hsiao, B. S.; Gardner, K. H.; Wu, D. Q.; Chu, B. Time-resolved X-ray study of poly(aryl ether ether ketone) crystallization and melting behaviour: 1. Crystallization. *Polymer* **1993**, *34*, 3986−3995.
(47) Benedetti, L.; Brulé, B.; Decraemer, N.; Davies, R.; Evans, K. E.; Ghita, O. A route to improving elongation of high-temperature laser sintered PEKK. *Addit. Manuf.* **2020**, *36*, 101540.
(48) Yi, N.; Davies, R.; Chaplin, A.; McCutchion, P.; Ghita, O. Slow and fast crystallising poly aryl ether ketones (PAEKs) in 3D printing: Crystallisation kinetics, morphology, and mechanical properties. *Addit. Manuf.* **2021**, *39*, 101843.
(49) Choupin, T.; Fayolle, B.; Régnier, G.; Paris, C.; Cinquin, J.; Brulé, B. Isothermal crystallization kinetic modeling of poly(etherketoneketone) (PEKK) copolymer. *Polymer* **2017**, *111*, 73−82.
(50) Chen, P.; Su, J.; Wang, H.; Yang, L.; Li, M.; Li, Z.; Liu, J.; Wen, S.; Zhou, Y.; Yan, C.; Shi, Y. Aging mechanism of polyetheretherketone powder during layer-wise infrared radiation of high-temperature laser powder bed fusion. *Mater. Des.* **2022**, *213*, 110348.
(51) Goodridge, R. D.; Tuck, C. J.; Hague, R. J. M. Laser sintering of polyamides and other polymers. *Prog. Mater. Sci.* **2012**, *57*, 229−267.
(52) Berretta, S.; Evans, K. E.; Ghita, O. R. Predicting processing parameters in high temperature laser sintering (HT-LS) from powder properties. *Mater. Des.* **2016**, *105*, 301−314.
(53) Chen, P.; Cai, H.; Li, Z.; Li, M.; Wu, H.; Su, J.; Wen, S.; Zhou, Y.; Liu, J.; Wang, C.; Yan, C.; Shi, Y. Crystallization kinetics of polyetheretherketone during high temperature-selective laser sintering. *Addit. Manuf.* **2020**, *36*, 101615.
(54) Brulé, B.; Decraemer, N., Method for producing an object by melting a polymer powder in a powder sintering device. US Patent 10,322,542 B2, (accessed June 18, 2019).